

Optimal Utilization Strategy of the LiFePO₄ Battery Storage

Timur Sayfutdinov^{a,b,*}, Petr Vorobev^a

^a*Center for Energy Science and Technology, Skolkovo Institute of Science and Technology, 3 Nobel Street, Skolkovo, Moscow Region 121205, Russia*

^b*School of Engineering, Newcastle University, Newcastle upon Tyne, United Kingdom*

Abstract

The paper provides a comprehensive battery storage modelling approach, which accounts for operation- and degradation-aware characteristics, i.e., variable efficiency, internal resistance growth, and capacity fade. Based on the available experimental data from the literature, we build mixed-integer linear programming compatible lithium iron phosphate (LiFePO₄) battery model that can be used in problems related to various applications, i.e., power system, smart grid, and vehicular applications. Such formulation allows finding the globally optimal solution using off-the-shelf academic and commercial solvers. In the numerical study, the proposed modelling approach has been applied to realistic scenarios of peak-shaving, where the importance of considering the developed models is explicitly demonstrated. For instance, a time-varying operation strategy is required to obtain the optimal utilization of the LiFePO₄ battery storage. Particularly, during the battery operational lifetime its optimal average SoC may change by up to 20%, while the duration of charging process may increase by 75%. Finally, using the same LiFePO₄ benchmark model from the literature, we compare the results of using the proposed approach to the state-of-the-art in the optimal sizing and scheduling problems. The proposed approach led to a 12.1% reduction of battery investment and operating costs compared to the state-of-the-art method.

Keywords: Lithium-ion batteries, Mixed-integer linear programming, Optimal scheduling

*timur.sayfutdinov@skolkovotech.ru

1. Introduction

Nowadays, energy storage systems have established their efficacy for more than a dozen power system applications, which cover all stages in the energy supply chain: bulk power and energy; ancillary services; transmission and distribution infrastructure applications; customer energy management [1]. Among all storage technologies used in power systems, lithium-ion (Li-ion) batteries are the fastest-growing energy storage technology [2], which is characterized by high efficiency, high power and energy density, long cycle lifetime, and environmental friendliness [3]. As with any other equipment utilized in power systems, a techno-economic analysis should be performed for Li-ion storage systems prior to its installation and operation, which is usually done employing various optimization methods [4]. The result of such an analysis is typically an optimal choice for storage unit siting, sizing, and technology selection as well as the optimal charge/discharge scheduling, i.e., operation strategy.

In early optimization problem formulations, such as in [5, 6], constant efficiency for charge and discharge were considered when modelling battery behavior. In practice, efficiency is a function of the battery output current, and also the battery state parameters, which include internal resistance and open-circuit voltage, that change significantly with the battery State of Charge (SoC), temperature, and State of Health (SoH) [7]. For instance, it was shown in [8] that charge and discharge efficiencies may vary significantly - they can drop as much as 33% from their maximum values depending on the battery operating conditions. To account for the influence of power output and SoC on battery efficiency, [9] proposed a second-order polynomial formulation, which can be considered within the convex programming approach. Then, a Mixed-Integer Linear Programming (MILP) compatible representation of the Li-ion battery has been proposed in [10], where efficiency was modelled using a piece-wise linear approximation of the simulated sample data. As an efficient alternative, [8] proposed a Linear Programming (LP) framework to account for efficiency based on the equivalent circuit model, while still considering the MILP formulation in [10] as a benchmark.

While focusing on a more accurate representation of battery efficiency, the above mentioned references did not account for an *operation-aware lifetime* and, most importantly, for the *available energy capacity* of the Li-ion battery storage, which decreases gradually over its lifetime due to degradation. The very first attempts to represent operation-aware battery lifetime

were models based on the total energy throughput, as in [11]. To respect the nonlinear relationship between battery operation strategy, i.e., Depth of Discharge (DoD), and its cycle lifetime, [12] approximated the dependency using a piece-wise linear formulation and considered it within a MILP framework for optimal battery sizing problem. Next, in [13] previous approaches were enhanced by incorporating C -rate as an additional factor of battery wear-and-tear. However, the methods above did not account for inevitable capacity loss of Li-ion battery over its lifetime, which plays one of the most important roles in techno-economic analysis of battery storage.

Extensive experimental results [14, 15, 16, 17, 18] suggest that the battery degradation depends in a more complicated (often non-linear) way on a number of factors, such as battery SoC, temperature, DoD etc. Thus, certain approximations have to be made to account for these effects when formulating an optimization problem for techno-economical analysis. In early attempt [19], a constant capacity fade rate of Li-ion battery was introduced for the storage investment problem. Even though the degradation rate was considered to be fixed, irrespective of the battery operation, the results suggest that capacity fade is among the most important factors to account for. In addition to the previous effect, in [20, 21] the battery available capacity was considered to be fading in time proportionally to the energy throughput. Considering the degradation rate to be dependant on operation variables, i.e., battery power output, made the optimization problem bilinear and required applying the whole enumeration search to find the globally optimal solution. In our recent study [22], a dynamic programming and mixed-integer problem reformulation approaches have been proposed to consider operation-aware degradation from SoC and DoD, while still respecting the formal optimization requirements. In [23], the short-term operation strategy of the Li-ion battery storage has been investigated using the MILP problem formulation, where the nonlinear cycling degradation effect from SoC, DoD and C -rate has been captured using the piece-wise linear approximation. In [24, 25], comprehensive Li-ion battery models were formulated for the optimal sizing problem, where the capacity fade effect from both idling and cycling mechanisms were complemented with the phenomenon known as the internal resistance growth, which affects the battery maximum power output and efficiency. Both models are characterized with the nonlinear formulation, which were approached with two distinct methods. Particularly, the Particle Swarm Optimization heuristic has been used in [24], while a formal approach of dynamic programming has been applied in [25], where the former method

cannot guarantee optimality of a solution and the latter possesses high computational burden.

In contrast to the previous references, we develop a comprehensive battery modelling approach that takes into account a variety of physical phenomena and can be used in a MILP problem formulation that allows finding the globally optimal solution in a computationally efficient way. Based on the existing experimental literature, we propose lithium iron phosphate (LiFePO_4) battery model that include the realistic dependencies of efficiency, lifetime, and available capacity on its operation strategy and linearize them using the *Special Order Sets 2*. We then provide the formulation of an optimization problem for the optimal choice of battery size and operation strategy for realistic case-studies, where the operation strategy can be adjusted for each battery lifetime period individually, i.e., optimization problem variables. Our findings suggest that there exist a number of trade-offs when deciding on a particular battery size and operation strategy, where the former might be significantly bigger than the minimum required capacity and the latter should be modified over the whole battery lifetime to provide economically optimal result. Particularly, to achieve optimal utilization of the LiFePO_4 battery, its capacity may exceed the minimum service requirement by at least 77.3%, its average SoC needs to be altered by up to 20%, while the duration of charging process is required to increase by up to 75% during the battery lifetime. The associated economical effect of the proposed approach, compared to the state-of-the-art methodology, accounts for 12.1% of reduction of battery investment and operating costs. Even though the proposed approach has been demonstrated for the LiFePO_4 battery, the methodology is applicable for other types of Li-ion family.

To summarize, the main contributions of the present manuscript are the following:

1. A MILP compatible battery model that is based on the experimental results on Li-ion technology and accounts for realistic operation-aware efficiency and degradation, including capacity fade and internal resistance growth.
2. We illustrate that the LiFePO_4 battery operation strategy requires significant life-long modifications to achieve the optimal battery utilization.
3. We validate our findings on real case-studies and demonstrate that there exist a number of trade-offs in LiFePO_4 battery operation, which

impact the operation strategy.

2. Li-ion Battery Modelling

The central part in energy storage modelling is a storage continuity differential equation, which tracks the battery charge. In a general form, it looks as follows

$$\dot{e} = P^B, \quad (1)$$

where e is a battery charge and P^B is a battery power input. While the former cannot take negative values, the latter is positive when the battery charges and negative when it discharges.

The battery power input P^B accounts for the amount of power drawn in and out of the battery cells. Due to power losses, present in real cells, the battery power input P^B is different from the power seen at terminals P^T - power that goes to/from the grid. In the most simplistic representation, the ratio of P^B and P^T is considered to be constant, which corresponds to constant battery efficiency. In reality, the efficiency depends on the battery operation parameters as well as on its SoH. In the present study, we use the equivalent circuit representation to approximate the relationship between P^B and P^T .

2.1. Equivalent circuit model

Equivalent circuit modelling is an efficient tool to represent complex phenomena using circuit theory. A comprehensive electric circuit model for Li-ion cells derived from physics-based phenomenological model has been provided in [26]. The model incorporates a number of *RLC* circuits connected in series that represent dynamics of electrochemical processes, and it is mainly used for dynamic studies. However, due to non-linearity such detailed model is found to be intractable for optimization tasks. In fact, this detalization is found to be redundant for the applications where the time-scale is significantly longer than the transient time constant, i.e., scheduling and sizing. Thus, given the fact that the aggregate time constant of transient processes of Li-ion batteries is in the order of minutes [7], a steady-state model can be effectively used for the optimal siting and scheduling problems, where the characteristic time-scale is of the order of hours or half-hours. The equivalent steady-state model would correspond to a circuit that contains voltage source and effective series resistance as depicted in Fig. 1 - *Rint* model [27].

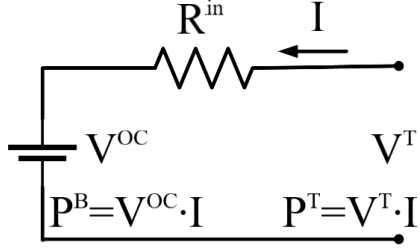


Figure 1: Rint model of a Li-ion cell

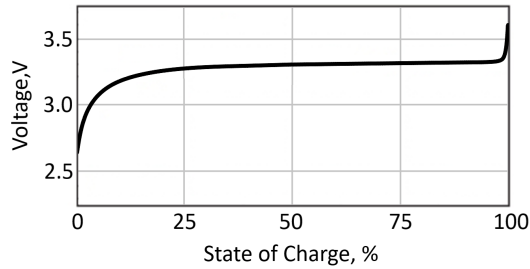


Figure 2: LiFePO₄ battery open-circuit voltage vs SoC

Given the *Rint* model of Fig. 1, the battery power input P^B can be expressed as a function of the power at terminals P^T and battery state parameters, i.e., open-circuit voltage V^{OC} and internal resistance R^{in} ,

$$P^B = \frac{V^{OC} \sqrt{V^{OC^2} + 4P^T R^{in}} - V^{OC^2}}{2R^{in}}. \quad (2)$$

The first element of the *Rint* model is a voltage source, with voltage level V^{OC} dependent on the battery SoC. Fig. 2 illustrates the dependency of the LiFePO₄ battery open-circuit voltage and SoC state value at 25°C [7]. For Li-ion chemistries, the dependency is considered to be linear within a wide range of SoC. Particularly, for LiFePO₄ batteries it is found to be linear between 10% and 98% SoC. Thus, it can be effectively approximated using the following linear relation:

$$V^{OC}(SoC) = k^V SoC + V^0, \quad (3)$$

where k^V is a voltage slope and V^0 is an offset value, e.g., for LiFePO₄ battery $k^V = 0.15$ V/pu, $V^0 = 3.2$ V.

The second element of the *Rint* model is the internal resistance R^{in} , which incorporates a series of resistive elements of the original model [26]

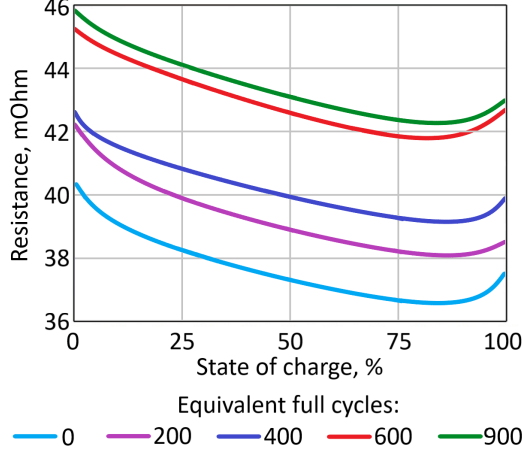


Figure 3: Resistance vs SoC

and depend on the state of the battery, including SoC and SoH, where the latter sometimes is expressed in the equivalent full cycles. Fig. 3 illustrates the relationship of the internal battery resistance from SoC and the number of equivalent full cycles at 25°C [15]. It can be noted that the value of the internal resistance is a non-monotonous function of SoC, which can be effectively linearized using three linear segments. At the same time, the value of internal resistance increases monotonously with the equivalent full cycles and can be approximated with a single linear function. Thus, the battery internal resistance can be represented with the combination of linear functions as follows:

$$R^{\text{in}} = \sum_{k=1}^K (a_k^{\text{SoC}} \text{SoC}_k + b_k^{\text{SoC}}) + a^{\text{FC}} N^{\text{FC}}, \quad (4)$$

where SoC_k is the k -th segment of the battery SoC, a_k^{SoC} and b_k^{SoC} are the corresponding coefficients of the linear functions, a^{FC} is a rate of internal resistance growth, and N^{FC} is a number of equivalent full cycles. The latter is found as a ratio of energy throughput to double capacity.

To estimate the losses obtained by the proposed *Rint* model and the dependencies above, the charge and discharge efficiencies can be found as a ratio between P^{B} and P^{T} , depending on the power flow direction. Fig. 4 illustrates battery discharge efficiencies derived from (2) for RCR123A 0.45Ah LiFePO₄ cell from [26] at the beginning of its lifetime. It can be noted that

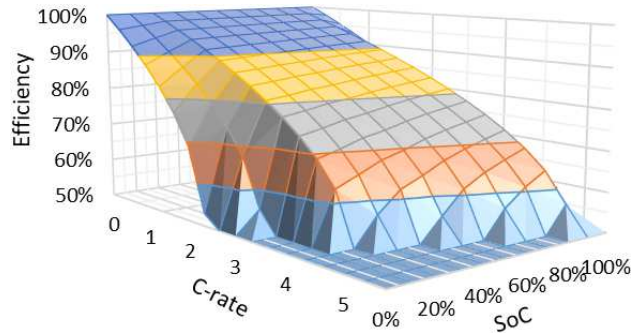


Figure 4: Discharge efficiency vs SoC and C-rate

even at a moderate discharge rate of 1C, one-way efficiency may drop below 90%.

2.2. Degradation model

From the operational perspectives, the most important aspects of the Li-ion battery degradation are internal resistance growth and capacity fade. While the former influences the maximum power output and losses, the latter affects the available energy capacity during the battery lifetime.

The battery internal resistance growth is associated with the Solid Electrolyte Interface (SEI) formation on the surface of the anode [14]. The SEI resistance increases with every cycle through the whole battery lifetime, which is considered by the second term in (4). As reported in [15], the total internal resistance increases nearly linearly with the number of equivalent full cycles, rising by as much as 20% per 1,000 full cycles.

The next aspect of the battery degradation is a continuous decrease of available capacity - capacity fade. There are two main degradation mechanisms considered in the literature, namely, idling δ^{idl} and cycling δ^{cyc} , and the total capacity loss δ^{CF} can be approximated as a sum of both contributions [28]:

$$\delta^{\text{CF}} \approx \delta^{\text{idl}} + \delta^{\text{cyc}}. \quad (5)$$

Degradation from cycling implies that the available capacity decreases after each charge-discharge cycle, and the amount of the capacity loss is driven by the charge and discharge rate (C-rate), cycle DoD and SoC range, and cell temperature during the cycle [18]. At the same time, idling degradation implies that the available capacity is lost, even when the battery is not being cycled. The rate of capacity fade in this case depends on the state of the

battery, i.e., SoC and cell temperature [17]. In [18], empirical capacity fade models due to both cycling and idling are provided based on the accelerated aging tests results:

$$\delta^{\text{cyc}} = 0.00568e^{-1.943SoC^{\text{cyc}}} DoD^{0.7162} \sqrt{n}, \quad (6)$$

$$\delta^{\text{idl}} = 0.000112e^{0.7388SoC^{\text{idl}}} \tau^{0.8}, \quad (7)$$

where SoC^{cyc} is the SoC level around which a cycle is made, i.e., median cycle SoC, DoD is the cycle DoD, n is the number of cycles, SoC^{idl} is the average battery SoC and τ is time in days.

It can be noted that both (6) and (7) are formulated for the cell temperature of 25°C, which is considered to be constant in our study. The reason for that is two-fold. First, the battery thermodynamics depend on many application and chemistry agnostic factors, including ambient conditions, battery system form factor, and design of a cooling system. Second, most of the battery storage applications correspond to the C-rate, which does not exceed one, meaning that power losses are moderate and they do not influence cell temperature significantly [29].

Figs. 5 and 6 depict the capacity fade characteristics of the LiFePO₄ battery due to idling and cycling respectively, both assuming constant cell temperature of 25 °C. Particularly, Fig. 5 illustrates that capacity fade from idling is slower when the battery SoC is kept low. From this figure, one can infer that it is in general better to keep the battery discharged when the service is not required. On the other hand, Fig. 6 suggests that capacity loss from cycling is the most severe for high DoD and low median SoC. Thus, to decrease capacity loss from cycling, one would want to charge and discharge the battery around the highest possible SoC. Obviously, the above degradation mechanisms disagree and require a balanced trade-off to ensure optimal battery utilization.

3. Optimization Problem Formulation

In the present section we formulate a generic optimization problem for the optimal scheduling and sizing of Li-ion battery storage, which takes into account phenomena formulated in the previous section, and the battery is aimed to deliver power according to predetermined demand profiles, e.g.,

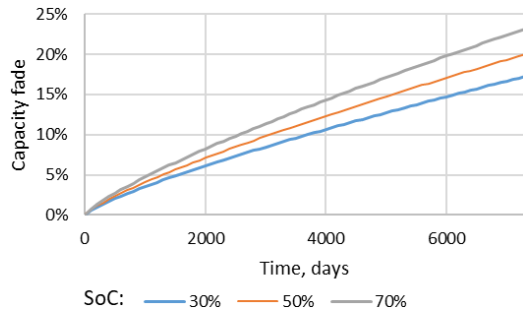


Figure 5: Capacity fade due to idling

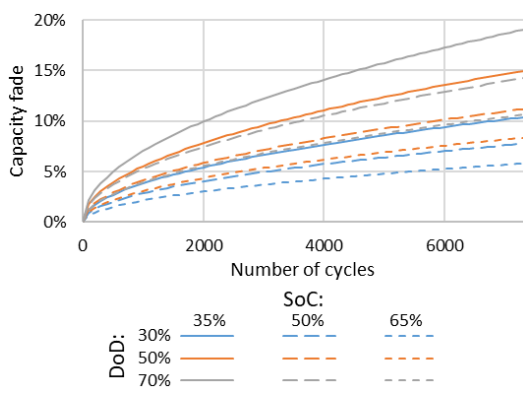


Figure 6: Capacity fade due to cycling

peak-shaving, EV drive cycle, etc. The corresponding objective function is formulated as follows

$$\min\left[\frac{C^E\bar{E} + C^P\bar{P}}{365 T^{\text{Lt}}} + \sum_{y \in Y} \pi_y \sum_{t \in T} (-C^{\text{LL}}P_{y,t}^{\text{LL}} + C^{\text{En}}(P_{y,t}^{\text{TCh}} + P_{y,t}^{\text{TDis}}))\Delta t\right], \quad (8)$$

where Y is a set of operation scenarios (e.g., years) indexed by y , T is a set of time intervals indexed by t with a time step Δt . π_y is a normalized probability of a scenario y . \bar{E} and \bar{P} are installed energy and power capacities of the battery, C^E and C^P are the corresponding prices for the installed capacities, which all together make the investment cost of energy storage. To consider the investment cost in the same time-scale as the daily operating costs, the later is divided by the battery lifetime $365 T^{\text{Lt}}$, which also corresponds to a planning horizon. The battery power input at terminals is broken into positive charge $P_{y,t}^{\text{TCh}}$ and negative discharge $P_{y,t}^{\text{TDis}}$ to avoid nonlinear problem formulation. C^{En} is a price for energy, necessary to translate power losses accounted in (2) into pecunial losses. $P_{y,t}^{\text{LL}}$ is a slack variable to allow minor deviations from the power balance equality (9), which is penalized by the value of lost load C^{LL} .

To ensure that the battery delivers power according to predetermined demand profiles, the following power balance and thermal line limit constraints are applied

$$P_{y,t}^{\text{G}} + P_{y,t}^{\text{D}} + P_{y,t}^{\text{TCh}} + P_{y,t}^{\text{TDis}} + P_{y,t}^{\text{LL}} = 0, \quad (9)$$

$$-\bar{P}^{\text{G}} \leq P_{y,t}^{\text{G}} \leq 0, \quad (10)$$

where $P_{y,t}^{\text{G}}$ is a power supplied from the grid, \bar{P}^{G} is the line thermal limit and $P_{y,t}^{\text{D}}$ is a power demand profile.

To model battery storage, the linear and mixed-integer linear constraints are formulated below. First, storage continuity differential equation (1) in a discrete form looks as follow

$$e_{y,t+1} = (1 - k^{\text{sd}})e_{y,t} + (P_{y,t}^{\text{BCh}} + P_{y,t}^{\text{BDis}})\Delta t, \quad (11)$$

where k^{sd} is a self-discharge rate and battery power input P^{B} from (2) is broken into positive charge $P_{y,t}^{\text{BCh}}$ and negative discharge $P_{y,t}^{\text{BDis}}$ to avoid nonlinear problem formulation.

Net storage charge, power rating, available storage capacity and maximum capacity fade are respected through (12) - (16)

$$e_{y,1} = e_{y,T+1}, \quad (12)$$

$$0 \leq P_{y,t}^{\text{TCh}} \leq \bar{P}, \quad (13)$$

$$-\bar{P} \leq P_{y,t}^{\text{TDis}} \leq 0, \quad (14)$$

$$0 \leq e_{y,t} \leq \bar{E}(1 - \delta_y^{\text{CF}}), \quad (15)$$

$$\delta_y^{\text{CF}} \leq 1 - \text{EoL}, \quad (16)$$

where δ_y^{CF} is a battery capacity fade and EoL is End of Life criterion, i.e., minimum remaining battery capacity threshold.

Before approximating nonlinear battery power input and capacity fade using *Special Order Sets 2* it is required that the reference variables are broken into segments as in (17)-(22)

$$P_{y,t}^{\text{TCh}} = \sum_{g=1}^{\text{G}} P_{y,t,g}^{\text{TCh}}, \quad (17)$$

$$P_{y,t}^{\text{TDis}} = \sum_{h=1}^{\text{H}} P_{y,t,h}^{\text{TDis}}, \quad (18)$$

$$\frac{1}{2\bar{E}} \sum_{t \in T_c} (P_{y,t}^{\text{BCh}} - P_{y,t}^{\text{BDis}}) \Delta t = \sum_{i=1}^{\text{I}} DoD_{y,c,i}^{\text{cyc}} \quad (19)$$

$$\frac{\min_{t \in T_c} \{e_{y,t}\}}{\bar{E}} + \frac{\sum_{i=1}^{\text{I}} DoD_{y,c,i}^{\text{cyc}}}{2} = \sum_{l=1}^{\text{L}} SoC_{y,c,l}^{\text{cyc}}, \quad (20)$$

$$\frac{1}{\bar{E}T} \sum_{t \in T} e_{y,t} \Delta t = \sum_{j=1}^{\text{J}} SoC_{y,j}^{\text{idl}}, \quad (21)$$

$$\frac{e_{y,t}}{\bar{E}} = \sum_{k=1}^{\text{K}} SoC_{y,t,k}, \quad (22)$$

where segmented $P_{y,t,g}^{\text{TCh}}$ and $P_{y,t,h}^{\text{TDis}}$ are charge and discharge power outputs, $DoD_{y,c,i}^{\text{cyc}}$ and $SoC_{y,c,l}^{\text{cyc}}$ are cycle DoD and median SoC, $SoC_{y,j}^{\text{idl}}$ is the average daily SoC and $SoC_{y,t,k}$ is momentary SoC. T_c is a time range of a cycle c ,

T_c is a cycle duration and G, H, I, J, K, L are the numbers of segments. In (20), the minimum battery charge during a cycle is found with the following reformulation

$$\min_{t \in T_c} \{e_{y,t}\} = e_{y,c}^{\min}, \quad (23)$$

$$e_{y,c}^{\min} \leq e_{y,t} \quad \forall t \in T_c. \quad (24)$$

To ensure that the segments in (17)-(22) are filled in the consecutive manner, the following constraints are applied

$$|P_g^{\text{TCh}}| \alpha_{y,t,g+1} \leq P_{y,t,g}^{\text{TCh}} \leq |P_g^{\text{TCh}}| \alpha_{y,t,g}, \quad g = 1..G, \quad (25)$$

$$|P_h^{\text{TDis}}| \beta_{y,t,h+1} \leq P_{y,t,h}^{\text{TDis}} \leq |P_h^{\text{TDis}}| \beta_{y,t,h}, \quad h = 1..H, \quad (26)$$

$$|\text{DoD}_i^{\text{cyc}}| \gamma_{y,c,i+1} \leq \text{DoD}_{y,c,i}^{\text{cyc}} \leq |\text{DoD}_i^{\text{cyc}}| \gamma_{y,c,i}, \quad i = 1..I, \quad (27)$$

$$|\text{SoC}_l^{\text{cyc}}| \zeta_{y,c,l+1} \leq \text{SoC}_{y,c,l}^{\text{cyc}} \leq |\text{SoC}_l^{\text{cyc}}| \zeta_{y,c,l}, \quad l = 1..L, \quad (28)$$

$$|\text{SoC}_j^{\text{idl}}| \eta_{y,j+1} \leq \text{SoC}_{y,j}^{\text{idl}} \leq |\text{SoC}_j^{\text{idl}}| \eta_{y,j}, \quad j = 1..J, \quad (29)$$

$$|\text{SoC}_k| \theta_{y,t,k+1} \leq \text{SoC}_{y,t,k} \leq |\text{SoC}_k| \theta_{y,t,k}, \quad k = 1..K, \quad (30)$$

where $\alpha_{y,t,g}, \beta_{y,t,h}, \gamma_{y,c,i}, \zeta_{y,c,l}, \eta_{y,j}, \theta_{y,t,k}$ are auxiliary binary variables, which indicate if a particular segment is used, and the binaries for the indices $G + 1, H + 1, I + 1, J + 1, K + 1, L + 1$ are enforced to zeros and considered as parameters. Finally, $|\cdot|$ is a length of a particular segment.

Now capacity fade can be approximated as follows

$$\begin{aligned} \delta_{y+1}^{\text{CF}} = \delta_y^{\text{CF}} + \sum_{c=1}^C \left[\sum_{i=1}^I (\gamma_{y,c,i} - \gamma_{y,c,i+1}) \sum_{l=1}^L (\zeta_{y,c,l} - \zeta_{y,c,l+1}) \right. \\ \left. \cdot \frac{\partial \delta^{\text{cyc}}(\hat{\text{DoD}}_{y,c,i}^{\text{cyc}}, \hat{\text{SoC}}_{y,c,l}^{\text{cyc}}, 365C(y - 0.5))}{\partial n} \right] + \\ + \sum_{j=1}^J (\eta_{y,j} - \eta_{y,j+1}) \frac{\partial \delta^{\text{idl}}(\hat{\text{SoC}}_{y,j}^{\text{idl}}, 365(y - 0.5))}{\partial \tau} \cdot 365, \quad (31) \end{aligned}$$

where C is a number of cycles performed during a scenario. The partial derivatives of capacity fade from cycling (6) and idling (7) are found for the corresponding lifetime moments, i.e, time, number of performed cycles, cycle DoD $\hat{\text{DoD}}_{y,c,i}^{\text{cyc}}$, median cycle SoC $\hat{\text{SoC}}_{y,c,l}^{\text{cyc}}$ and average daily SoC $\hat{\text{SoC}}_{y,j}^{\text{idl}}$. The

latter three are found as follows

$$\hat{\text{DoD}}_{y,c,i}^{\text{cyc}} = \sum_{i'=1}^{i-1} |\text{DoD}_{i'}^{\text{cyc}}| + \frac{|\text{DoD}_i^{\text{cyc}}|}{2}, \quad (32)$$

$$\hat{\text{SoC}}_{y,c,l}^{\text{cyc}} = \sum_{l'=1}^{l-1} |\text{SoC}_{l'}^{\text{cyc}}| + \frac{|\text{SoC}_l^{\text{cyc}}|}{2}, \quad (33)$$

$$\hat{\text{SoC}}_{y,j}^{\text{idl}} = \sum_{j'=1}^{j-1} |\text{SoC}_{j'}^{\text{idl}}| + \frac{|\text{SoC}_j^{\text{idl}}|}{2}. \quad (34)$$

The product of binary variables in (31) is substituted with a variable $u_{y,c,i,l} = \gamma_{y,c,i} \zeta_{y,c,l}$, which is linearized as in (35)

$$\begin{aligned} 0 &\leq u_{y,c,i,l} \leq 1, \\ u_{y,c,i,l} &\leq \gamma_{y,c,i}, \\ u_{y,c,i,l} &\leq \zeta_{y,c,l}, \\ u_{y,c,i,l} &\geq \gamma_{y,c,i} + \zeta_{y,c,l} - 1. \end{aligned} \quad (35)$$

Next, charge and discharge battery power output is approximated as follows

$$\begin{aligned} P_{y,t}^{\text{BCh}} &= \prod_{y'=1}^y \sum_{i=1}^I (\gamma_{y',c,i} - \gamma_{y',c,i+1}) \sum_{k=1}^K (\theta_{y,t,k} - \theta_{y,t,k+1}) \\ &\quad \sum_{g=1}^G \frac{\partial P^{\text{B}}(\hat{P}_g^{\text{TCh}}, \hat{\text{SoC}}_{y,t,k}, \hat{N}_{I(y)}^{\text{FC}})}{\partial P^{\text{T}}} P_{y,t,g}^{\text{TCh}} \end{aligned} \quad (36)$$

$$\begin{aligned} P_{y,t}^{\text{BDis}} &= \prod_{y'=1}^y \sum_{i=1}^I (\gamma_{y',c,i} - \gamma_{y',c,i+1}) \sum_{k=1}^K (\theta_{y,t,k} - \theta_{y,t,k+1}) \\ &\quad \sum_{h=1}^H \frac{\partial P^{\text{B}}(-\hat{P}_h^{\text{TDis}}, \hat{\text{SoC}}_{y,t,k}, \hat{N}_{I(y)}^{\text{FC}})}{\partial P^{\text{T}}} P_{y,t,h}^{\text{TDis}} \end{aligned} \quad (37)$$

where the partial derivative of the battery power output (2) is found for each segment of terminal power outputs \hat{P}_g^{TCh} and \hat{P}_h^{TDis} , momentary SoC $\hat{\text{SoC}}_{y,t,k}$

and the number of full equivalent cycles $\hat{N}_{I(y)}^{\text{FC}}$, which are found as follows

$$\hat{P}_g^{\text{TCh}} = \sum_{g'=1}^{g-1} |P_{g'}^{\text{TCh}}| + \frac{|P_g^{\text{TCh}}|}{2}, \quad (38)$$

$$\hat{P}_h^{\text{TDis}} = \sum_{h'=1}^{h-1} |P_{h'}^{\text{TDis}}| + \frac{|P_h^{\text{TDis}}|}{2}, \quad (39)$$

$$\hat{\text{SoC}}_{y,t,k} = \sum_{k'=1}^{k-1} |\text{SoC}_{k'}| + \frac{|\text{SoC}_k|}{2}, \quad (40)$$

$$\hat{N}_{I(y)}^{\text{FC}} = \sum_{y'=1}^y \sum_{i'=1}^{i(y')-1} |\text{DoD}_{i'}^{\text{cyc}}| + \frac{|\text{DoD}_{i(y')}^{\text{cyc}}|}{2}, \quad (41)$$

where $I(y)$ is a set of segments used in a particular year y .

Finally, to linearize the product of binary and continuous variables in (36) and (37), the product of binary variables $\gamma_{1,c,I(1)} \cdot \gamma_{y,c,I(y)} \theta_{y,t,k} = v_{I(y),k}$ has been linearized similar to the previous instance

$$\begin{aligned} 0 &\leq v_{I(y),k} \leq 1, \\ v_{I(y),k} &\leq \gamma_{1,c,I(1)}, \dots \\ v_{I(y),k} &\leq \gamma_{y,c,I(y)}, \\ v_{I(y),k} &\leq \theta_{y,t,k}, \\ v_{I(y),k} &\geq \gamma_{1,c,I(1)} + \dots + \gamma_{y,c,I(y)} + \theta_{y,t,k} - y, \end{aligned} \quad (42)$$

while the products of binary and continuous variables $v_{I(y),k} P_{y,t,g}^{\text{TCh}} = w_{I(y),k,g}$ and $v_{I(y),k} P_{y,t,h}^{\text{TDis}} = x_{I(y),k,h}$ have been linearized as in (43) and (44), respectively

$$\begin{aligned} w_{I(y),k,g} &\leq |P_g^{\text{TCh}}| v_{I(y),k}, \\ P_{y,t,g}^{\text{TCh}} - |P_g^{\text{TCh}}| (1 - v_{I(y),k}) &\leq w_{I(y),k,g} \leq P_{y,t,g}^{\text{TCh}} \end{aligned} \quad (43)$$

$$\begin{aligned} x_{I(y),k,h} &\leq |P_h^{\text{TDis}}| v_{I(y),k}, \\ P_{y,t,h}^{\text{TDis}} - |P_h^{\text{TDis}}| (1 - v_{I(y),k}) &\leq x_{I(y),k,h} \leq P_{y,t,h}^{\text{TDis}} \end{aligned} \quad (44)$$

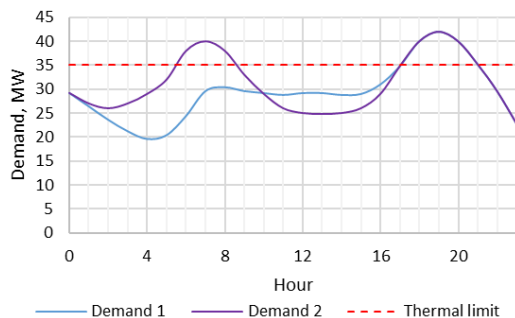


Figure 7: Case study demand profiles

4. Numerical Study

4.1. Case Study

For our particular examples we consider two peak-shaving scenarios, given by the Fig. 7, where blue and purple curves represent demand profiles with one and two peaks, respectively. The red dashed line represents the maximum desired demand level. Both cases illustrate practically wide-spread scenarios, where the first case can correspond to a typical evening peak situation [30], while the second - to a "duck curve" pattern due to massive photovoltaics integration [31]. In both cases, the minimum storage power and energy required to shave the highest peak are 7 MW and 17.2 MWh, respectively.

To focus on the optimal operation of the LiFePO_4 battery storage driven by its internal characteristics we fix external factors to constants, i.e., demand profiles remain unchanged during the battery lifetime and energy price C^{En} is fixed to 80 \$/MWh [32]. It is worth noting that the proposed approach allows considering variable energy price and a set of demand profiles for increasing load or stochastic problem formulation. Capital costs for battery power C^{P} and energy C^{E} capacities are 90 \$/kW and 290 \$/kWh, respectively [33]. The End of Life (EoL) criterion is set to 75%, while the planning horizon corresponds to the battery operational lifetime T^{Lt} , i.e., optimization problem variable.

4.2. Results

The main results of the formulated optimization problem applied to the case study above are provided in Table 1. For the one peak demand scenario, the optimal solution corresponds to 25.4MWh/7MW battery system, which

Table 1: Solutions of the optimization problem

Demand	Objective	Capacity	Lifetime
One peak	1512.1 \$/day	25.4 MWh / 7 MW	15 years
Two peak	2233.3 \$/day	30.5 MWh / 7 MW	12 years

results in per diem battery investment and operating costs of 1512.1\$/day for 15 years of operational lifetime. For the two peak demand scenario, the optimal solution suggests installing 30.5MWh/7MW battery storage, which corresponds to 2233.3\$/day of per diem battery investment and operating costs for 12 years of operation. Fig. 8 illustrates the maps of the objective function in battery storage capacity \bar{E} and operational lifetime T^{Lt} space for two demand scenarios, while Fig. 9 and 10 depict SoC, operation and degradation characteristics of the optimal solutions. Before analyzing the results, let us declare three major findings:

1. The optimal capacity of the LiFePO₄ battery is driven by the operating requirements, e.g., considerable capacity headroom becomes economically feasible for the case of two peaks per day.
2. Given the gradient near the optimal solutions in Fig. 8, it is safer to overestimate the capacity and underestimate operational lifetime than the opposite.
3. The operation strategy should be altered over the whole battery lifetime to ensure optimal utilization of the LiFePO₄ battery.

As it was already mentioned in the previous subsection, the minimum power and energy capacities to perform peak-shaving are 7 MW and 17.2 MWh, respectively. Even though, the optimal solutions match the minimum power capacity requirement, there exist significant headroom in terms of energy capacity. For instance, the optimal battery energy capacities for one and two peak demand scenarios (Table 1) correspond to 25.4 MWh and 30.5 MWh, which are 47.7% and 77.3% higher than the actual energy required to cover the highest peak, i.e., headroom. Even though, the large part of these (33.3%) corresponds to capacity fade compensation and around 2.5% can be attributed to compensate for discharge losses, the remaining capacity margin is related to the operation strategy. Particularly, for the one peak demand scenario, this accounts for the remaining 11.9% of energy capacity

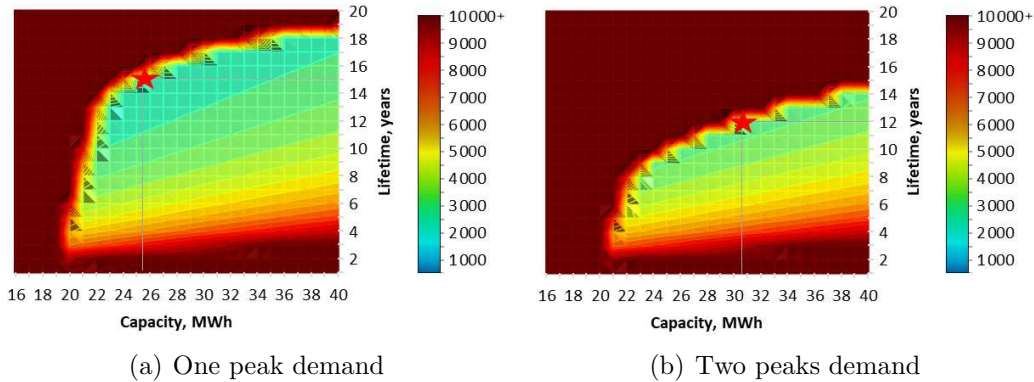


Figure 8: Objective function value as a function of installed energy capacity and operational lifetime

margin, while for the two peak demand scenario, where battery is used more extensively, this accounts for the remaining 41.5% of headroom to achieve optimal utilization of the LiFePO_4 battery storage. In contrast to the above solutions, a naive strategy would be to choose the battery capacity accounting only for the minimum required energy capacity, EoL criterion and discharge efficiency, e.g., $17.2 \text{ MWh} / 0.75 / 0.98 = 23.4 \text{ MWh}$. Even though the derived battery capacity would require less capital investments, compared to the obtained solutions, the resulting per diem investment and operating costs would be higher due to shorter operational lifetime (11 and 8 years for one peak and two peaks demand scenarios, respectively).

Fig. 8 illustrates the positions of the optimal solutions in the objective function value map, which is presented as a function of installed energy capacity and operational lifetime. The red stars indicate the minimum objective function value positions, i.e., the optimal solutions. For the one peak demand scenario (a), the minimum objective function value equals to 1512.1 \$/day, which corresponds to 25.4 MWh of installed energy capacity and 15 years of battery lifetime. For the two peak demand scenario (b), the minimum objective function value is found at the intersection of 30.5 MWh of installed energy capacity and 12 years of operational lifetime, and equals to 2233.3 \$/day. As it can be seen from Fig. 8, both solutions are located very close to the high gradient of the objective function, meaning that the small disturbance (error) of the optimal solution might result into significant increase of the objective function value. Particularly, the profitability

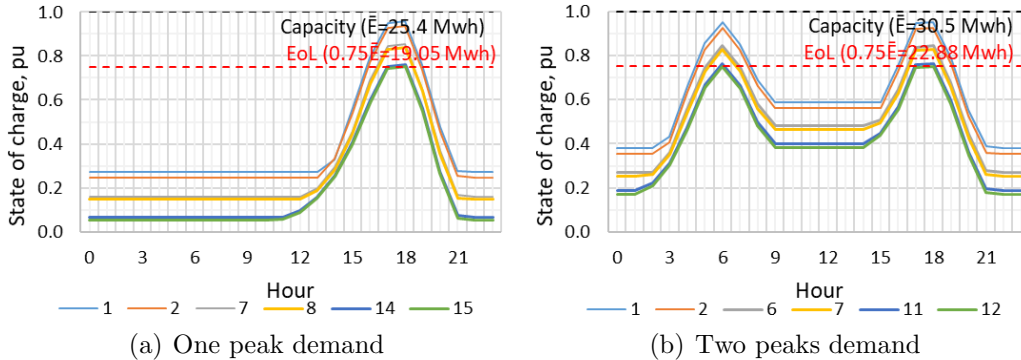


Figure 9: State of charge profiles of the optimal solution

of a solution might be significantly compromised if the capacity is underestimated and operational lifetime is overestimated. However, one might want to overestimate the installed energy capacity and underestimate operational lifetime to reduce the sensitivity and investment risks at the cost of a minor increase of the investment and operating costs.

Fig. 9 illustrates the optimal LiFePO_4 battery scheduling during the whole operational lifetime period. In case of the one peak demand scenario (a), the SoC profile variation changes from [27%;95.8%] range in the beginning of the battery lifetime to [5.4%;75%] during the terminal year. The similar picture is observed for the case of the two peak demand scenario (b), where the SoC ranges of two consecutive cycles change from [58.8%;95.2%] and [38%;95.2%] during the first year of operation to [38.4%;75%] and [17.3%;75%] during the terminal year, respectively. Even though the span of the ranges, i.e., DoD, increases only by 0.8% for the one peak demand scenario (a) and by 0.2% and 0.5% for the two consecutive peaks of the two peak demand scenario (b), the battery SoC strategy changes through the whole lifetime period quite significantly. For instance, the gradual decrease of the average battery SoC can be observed on Fig. 10, where in case of the one peak demand scenario (a) it drops from 39.3% to 19.1%, and in case of the two peak demand scenario (b) it falls from 61.8% to 42.1%. Since the DoD is tied to the amount of energy required to shave the peak, it cannot be changed once the battery capacity is chosen. Thus, the only operation characteristic that can be altered is the SoC, which is observed in the numerical study.

Given the constant peak-shaving requirements for the entire battery life-

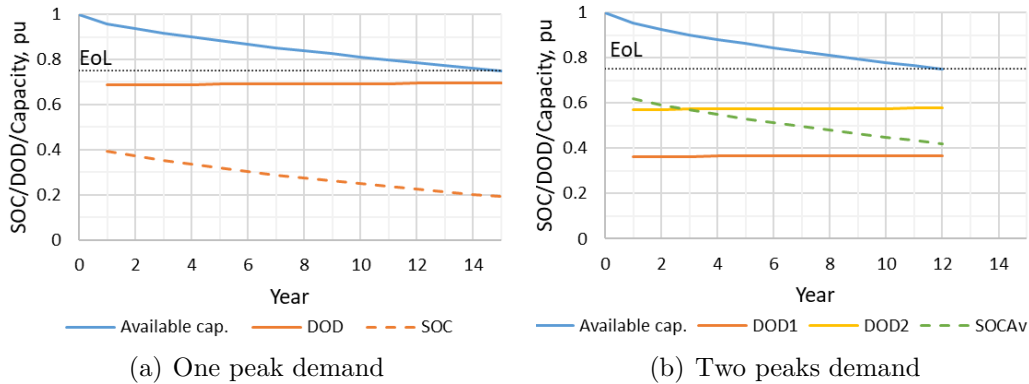


Figure 10: Operation and degradation characteristics of the optimal solution

time period, the small increase in the DoD strategy is explained by the need to compensate for the increased discharge losses associated with the internal resistance growth. The substantial alternation of the battery operation strategy relates to both internal resistance growth and capacity fade characteristics. As per (6) and (7), the battery SoC is in direct relation to the capacity fade from idling, while the median cycle SoC is in inverse relation to the capacity fade from cycling. Thus, on Fig. 9 we can observe a rapid charge of the battery just before it is required to discharge. This way it is possible to keep the average battery SoC low, while the median cycle SoC is high, which is complementary to slow degradation process. However, given the fact that the average daily SoC decreases asymptotically with the available capacity (see Fig. 10), it can be concluded that capacity fade from cycling is the dominating factor. Also, it can be noted that during the course of the battery lifetime, the time duration for battery charging is increased from four hours in the beginning of the battery lifetime to seven hours during the terminal year (see Fig. 9), which negatively affects the average daily SoC. This reflects the time-varying trade-off between power losses and capacity fade from idling, where the latter dominates during the early battery lifetime, while the former comes to the fore after.

4.3. Comparative analysis

To quantify the advantages of the proposed modelling approach, it has been compared to two existing battery sizing methodologies. The first methodology (referred to as "Cyc.Lt.(DoD,C-rate)") is taken from [13], where the

Table 2: Comparative study

Model	Objective	Capacity	Lifetime
Cyc.Lt.(DoD,C-rate)[13]	1879.5\$/day	23.4MWh/7MW	11years
Deg.(SoC,DoD,C-rate);Rint(SoC)[25]	1695.5\$/day	29.0MWh/7MW	15years
Proposed	1512.1\$/day	25.4MWh/7MW	15years

nonlinear relationship between the battery DoD, C-rate and cycle lifetime is considered with a piece-wise linear function. However, in opposite to the proposed methodology, the battery efficiency and available battery capacity are kept constant. The second methodology (referred to as "Deg.(SoC,DoD,C-rate);Rint(SoC)") has been proposed in [25], where the dynamic programming optimization is used to resolve a comprehensive Li-ion battery model that accounts for the battery degradation (i.e., capacity fade and internal resistance growth from both idling and cycling), and SoC dependant equivalent circuit *Rint* model. In contrast to the proposed approach, both methodologies allow choosing only one battery operation strategy for the whole planning horizon, while, as it has been shown in the previous subsection, to achieve optimal battery utilization the strategy needs to be substantially altered during the whole operational lifetime (see Fig. 9 and 10). All three methodologies have been applied to the same LiFePO₄ benchmark model from the literature and the same case-study of one peak demand scenario, described in the present section. It is worth noting that given the same disposition of the sizing methodologies to possible errors (investment risks), the obtained solutions would be indicative for the relative expected benefit of one method over the other if the original model is the same. Thus, we derive the advantage of the proposed methodology over the state-of-the-art based on the obtained optimal solutions.

The results of the three approaches under comparison are given in Table 2. In case of the variable battery lifecycle (Cyc.Lt.(DoD,C-rate)), the solution suggests installing 23.4MWh/7MW battery system, which results in daily investment and operating costs of 1879.5 \$/day. The optimal DoD is found to be 75%, which corresponds to the EoL criterion and leads to 4,000 cycles or 11 years. In case of the comprehensive battery modelling approach (Deg.(SoC,DoD,C-rate);Rint(SoC)), the optimal solution suggests installing

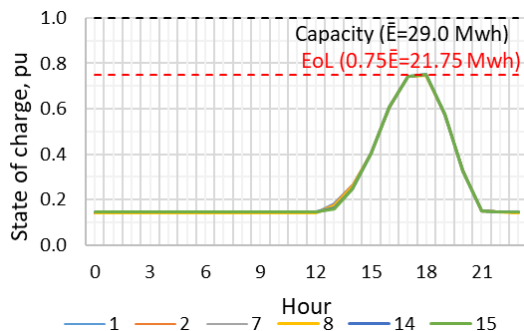


Figure 11: State-of-the-art solution [25] - State of charge profile

29.0MWh/7MW battery system, which results in the objective function value of 1695.5 \$/day. The solution corresponds to the battery dispatch depicted in Fig. 11, where the operation strategy is found to be 25.5% average battery SoC, 44.7% cycle median SoC, and 60.7% cycle DoD over the whole battery lifetime, which in this case is found to be 15 years. In its turn, the optimal solution obtained by the proposed approach corresponds to 25.4MWh/7MW battery system, which corresponds to the objective function value of 1512.1 \$/day for 15 years of expected battery lifetime. As per Fig. 9 (a) and 10 (a), the optimal battery utilization corresponds to the operation characteristics that evolve through the whole lifetime period. Particularly, the average battery SoC changes from 39.3% in the beginning of the battery lifetime to 19.1% during the terminal year, cycle median SoC changes from 61.4% to 40.2%, and cycle DoD changes from 68.8% to 69.6%. Compared to the previous approach, such adjustable operation strategy allows providing the same service for the same planning horizon with substantially smaller battery capacity. Particularly, the battery energy capacity found by the approach in [25] is 14.2% higher than the one found by the proposed method, what leads to 12.1% reduction of the objective function value, i.e., investment and operating costs.

5. Conclusions

This paper has presented a new battery modelling approach, which accounts for numerous Li-ion battery characteristics, i.e., degradation from idling and cycling, internal resistance as a function of both degradation and SoC, as well as the equivalent circuit model to account for battery efficiency. The nonlinear characteristics have been linearized using the *Special Order*

Sets 2 to be suitable for use within the MILP problems, e.g., optimal scheduling and sizing. The distinctive advantage of the proposed methodology resides in the fact that the operation strategy of a battery storage system can be adjusted for each lifetime period separately, i.e., separate variables of the optimization problem. Even though the proposed modelling approach have been based on the LiFePO_4 battery models available in the literature, the proposed methodology can be applied to other Li-ion chemistry.

Applying the developed LiFePO_4 battery model to realistic case-studies, it has been found that the optimal utilization of the battery corresponds to the nonconstant operation strategy through the whole battery lifetime. This includes increasing DoD to compensate for the growing internal resistance and associated charge and discharge losses, decreasing median cycle SoC to minimize battery degradation from cycling, and increasing average SoC and battery charging process duration as a trade-off between degradation from idling and growing charge and discharge losses. Finally, the proposed model have been applied to the optimal battery sizing problem and compared to the state-of-the-art methodologies, where an improvement of 12.1% in the investment and operating costs has been demonstrated.

References

- [1] A. Akhil, et al., DOE/EPRI 2013 electricity storage handbook in collaboration with NRECA, Sandia National Laboratories Albuquerque, NM, 2013.
- [2] Energy Storage Tracker 4Q19: Market Share Data, Industry Trends, Market Analysis, and Project Tracking by World Region, Technology, Application and Market Segment, Technical Report, Navigant Research, 2019.
- [3] X. Hu, et al., Technological developments in batteries: a survey of principal roles, types, and management needs, *IEEE Power and Energy Magazine* 15 (2017) 20–31.
- [4] M. Zidar, et al., Review of energy storage allocation in power distribution networks: applications, methods and future research, *IET Generation, Transmission & Distribution* 10 (2016) 645–652.
- [5] Y. Dvorkin, et al., Ensuring profitability of energy storage, *IEEE Transactions on Power Systems* 32 (2016) 611–623.

- [6] L. Xu, et al., Optimal sizing of plug-in fuel cell electric vehicles using models of vehicle performance and system cost, *Applied Energy* 103 (2013) 477–487.
- [7] G. L. Plett, *Battery management systems, Volume II: Equivalent-circuit methods, volume 2*, Artech House, 2015.
- [8] A. J. Gonzalez-Castellanos, et al., Non-ideal linear operation model for li-ion batteries, *IEEE Transactions on Power Systems* 35 (2020) 672–682.
- [9] T. Morstyn, et al., Model predictive control for distributed microgrid battery energy storage systems, *IEEE Transactions on Control Systems Technology* 26 (2018) 1107–1114.
- [10] A. Sakti, et al., Enhanced representations of lithium-ion batteries in power systems models and their effect on the valuation of energy arbitrage applications, *Journal of Power Sources* 342 (2017) 279–291.
- [11] T. Sayfutdinov, et al., Incorporating variable lifetime and self-discharge into optimal sizing and technology selection of energy storage systems 1 (2018) 11–18.
- [12] I. Alsaidan, et al., A comprehensive battery energy storage optimal sizing model for microgrid applications, *IEEE Transactions on Power Systems* 33 (2018) 3968–3980.
- [13] N. Padmanabhan, et al., Battery energy storage systems in energy and reserve markets, *IEEE Transactions on Power Systems* 35 (2020) 215–226.
- [14] S. Rodrigues, et al., Ac impedance and state-of-charge analysis of a sealed lithium-ion rechargeable battery, *Journal of Solid State Electrochemistry* 3 (1999) 397–405.
- [15] D. Wang, et al., Online lithium-ion battery internal resistance measurement application in state-of-charge estimation using the extended kalman filter, *Energies* 10 (2017) 1284.
- [16] R. Spotnitz, Simulation of capacity fade in lithium-ion batteries, *Journal of power sources* 113 (2003) 72–80.

- [17] S. Grolleau, et al., Calendar aging of commercial graphite/lifepo4 cell—predicting capacity fade under time dependent storage conditions, *Journal of Power Sources* 255 (2014) 450–458.
- [18] D. Stroe, et al., Degradation behavior of lithium-ion batteries based on lifetime models and field measured frequency regulation mission profile, *IEEE Transactions on Industry Applications* 52 (2016) 5009–5018.
- [19] T. Qiu, et al., Stochastic multistage coplanning of transmission expansion and energy storage, *IEEE Transactions on Power Systems* 32 (2017) 643–651.
- [20] I. Miranda, et al., A holistic approach to the integration of battery energy storage systems in island electric grids with high wind penetration, *IEEE Transactions on Sustainable Energy* 7 (2016) 775–785.
- [21] D. Parra, et al., Optimum community energy storage system for pv energy time-shift, *Applied Energy* 137 (2015) 576–587.
- [22] T. Sayfutdinov, et al., Degradation and operation-aware framework for the optimal siting, sizing and technology selection of battery storage, *IEEE Transactions on Sustainable Energy* (2019).
- [23] A. Maheshwari, et al., Optimizing the operation of energy storage using a non-linear lithium-ion battery degradation model, *Applied Energy* 261 (2020) 114360.
- [24] Y. Li, et al., Design of minimum cost degradation-conscious lithium-ion battery energy storage system to achieve renewable power dispatchability, *Applied Energy* 260 (2020) 114282.
- [25] A. Berrueta, et al., Combined dynamic programming and region-elimination technique algorithm for optimal sizing and management of lithium-ion batteries for photovoltaic plants, *Applied energy* 228 (2018) 1–11.
- [26] M. Greenleaf, et al., Application of physical electric circuit modeling to characterize li-ion battery electrochemical processes, *Journal of Power Sources* 270 (2014) 113–120.

- [27] T. Morstyn, et al., Scalable energy management for low voltage micro-grids using multi-agent storage system aggregation, *IEEE Transactions on Power Systems* 33 (2017) 1614–1623.
- [28] J. Schmalstieg, et al., A holistic aging model for li (nimmco) o2 based 18650 lithium-ion batteries, *Journal of Power Sources* 257 (2014) 325–334.
- [29] C. Patsios, et al., An integrated approach for the analysis and control of grid connected energy storage systems, *Journal of Energy Storage* 5 (2016) 48–61.
- [30] Customer-Led Network Revolution, Accessed 03-Apr-2020. <http://www.networkrevolution.co.uk/resources/project-data/>.
- [31] C. ISO, What the duck curve tells us about managing a green grid, Calif. ISO, Shap. a Renewed Futur (2012) 1–4.
- [32] Ofgem: Wholesale Market Indicators, Accessed 20-Dec-2020. <https://www.ofgem.gov.uk/data-portal/wholesale-market-indicators>.
- [33] R. Fu, T. W. Remo, R. M. Margolis, 2018 US utility-scale photovoltaics-plus-energy storage system costs benchmark, Technical Report, National Renewable Energy Lab.(NREL), Golden, CO (United States), 2018.

This figure "placeholder.jpg" is available in "jpg" format from:

<http://arxiv.org/ps/2101.11659v1>